minerals

MDPI

Article

Multi-Phase Hydrothermal Fluid Events in the Giant Lannigou Gold Deposit, SW China: Insights from Calcite Sm–Nd Age, Trace Elements, and C-O-Sr Isotopes

Piyou Li [1,2], Yuzhao Hu [1,2,*], Zhendong Tian [3], Shenjin Guan [1,2,*] and Huijun Fan [4]

[1] Faculty of Land Resource Engineering, Kunming University of Science and Technology, Kunming 650093, China; lpu_zd@163.com
[2] South-West Institute of Geological Survey, Geological Survey Center for Nonferrous Metals Resources, Kunming 650093, China
[3] State Key Laboratory of Ore Deposit Geochemistry, Institute of Geochemistry, Chinese Academy of Sciences, Guiyang 550081, China; tianzhendong@mail.gyig.ac.cn
[4] The First Gas Production Plant, PetroChina Changqing Oilfield Company, Jingbian 718500, China; 18049685948@163.com
* Correspondence: yuzhaohu@kust.edu.cn (Y.H.); guansj@kust.edu.cn (S.G.)

Abstract: The Nanpanjiang basin hosts the world's second-largest concentration of Carlin-type gold deposits. To decipher the origin and evolution of hydrothermal fluid, this study conducted Sm–Nd dating, in-situ trace element, and C-O-Sr isotopic analyses on three types of calcite samples from the giant Lannigou gold deposit in the Nanpanjiang basin, SW China. The type-I calcite, intergrown with Au-bearing arsenian pyrite, has an Sm–Nd isochron age of 213 ± 7 Ma (MSWD = 0.81), indicating that gold mineralization occurred in Late Triassic. The type-II calcite, which coexists with high-maturity bitumens and cut through the main-stage gold orebodies, yields an Sm–Nd age of 188 ± 14 Ma (MSWD = 0.34), representing a post-ore hydrocarbon accumulation event. The type-I and type-II calcite samples have low REE contents (5.28–51.6 ppm) and exhibit MREE-enriched and LREE-/HREE-depleted patterns. Combined with their identical C-O-Sr isotopes, we suggest that hydrothermal fluids responsible for the precipitation of type-I and type-II calcite samples were derived from a mixed metamorphic fluid and meteoric water source. In contrast, the type-III calcite samples, associated with realgar and orpiment, have distinct Mn, Sr, and As contents, REE patterns, and C-O-Sr isotopic composition from the type-I and II calcites, suggestive of different fluid sources. Based on our and previously published data, we propose that the fluid evolution, gold mineralization, and hydrocarbon accumulation in the Nanpanjiang basin are closely related to the Indosinian and Yanshanian orogenies in South China.

Keywords: calcite Sm–Nd age; C-O-Sr isotope; Lannigou gold deposit; Carlin-type gold deposit; Nanpanjiang basin

Citation: Li, P.; Hu, Y.; Tian, Z.; Guan, S.; Fan, H. Multi-Phase Hydrothermal Fluid Events in the Giant Lannigou Gold Deposit, SW China: Insights from Calcite Sm–Nd Age, Trace Elements, and C-O-Sr Isotopes. *Minerals* **2023**, *13*, 1420. https://doi.org/10.3390/min13111420

Academic Editor: Iuliu Bobos

Received: 21 September 2023
Revised: 1 November 2023
Accepted: 6 November 2023
Published: 8 November 2023

1. Introduction

Carlin-type gold deposits (CTDs) are sedimentary rock-hosted disseminated gold deposits that account for ~8% of annual worldwide Au production [1,2]. They were first discovered in Carlin, Nevada, USA in 1961. The Dian–Qian–Gui region is the world's second-largest CTD district (Figure 1), containing more than 200 gold deposits or occurrences with >800 tons of total proven Au reserves [3]. Recently, significant progress has been made in the metallogenic age [4–7], source of ore-forming materials [8–11], and metallogenic regularity [12–14] of these deposits. However, the nature and origin of ore-forming fluid for these deposits are highly debated [15–17], significantly hampering our understanding of the ore genesis of these deposits.

Calcite is a common mineral in hydrothermal deposits; its elemental and isotopic compositions record a wealth of information regarding fluid sources and evolution [18–20].

Moreover, Sm–Nd geochronology can be applied to constrain the timing of hydrothermal events [21–23]. The calcites in the CTDs of the Dian–Qian–Gui region are widely developed and closely associated with gold mineralization [24–26]. Thus, a systematic evaluation of calcite may provide critical insights into the nature and origin of the ore-forming fluid for CTDs.

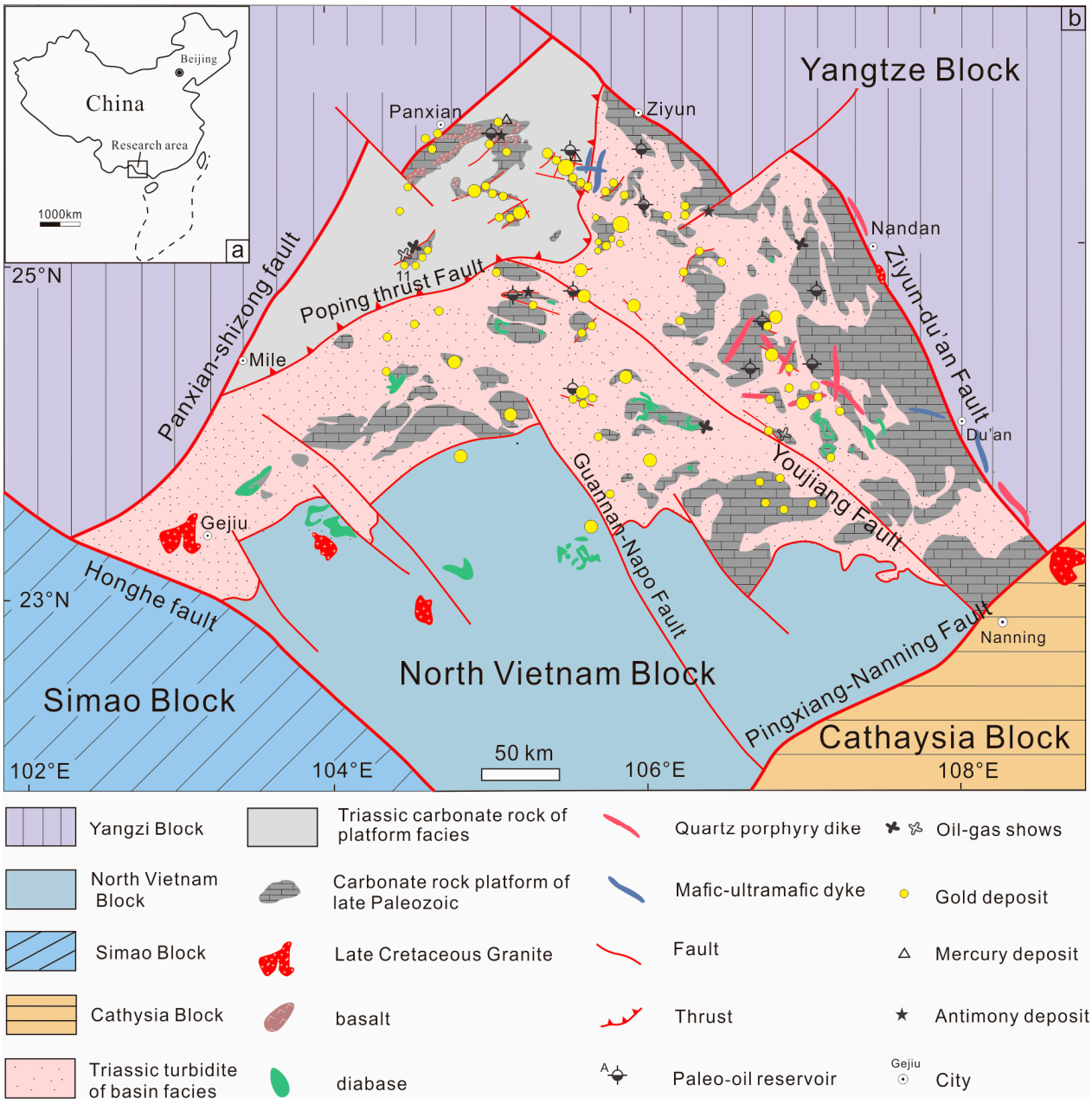

Figure 1. (**a**) Outline of China showing the location of the Nanpanjiang basin, (**b**) Simplified geological map of the major Carlin-type gold deposits in the Nanpanjiang basin (Modified from [27]).

The Lannigou gold deposit is one of the largest in the Dian–Qian–Gui area, containing 109 tons of Au reserves with an average 3.83 g/t grade [27]. In this study, three stages of calcite were identified in the deposit. Herein, we conducted in-situ trace element, rare earth element (REE), C-O-Sr isotope, and Sm–Nd geochronology analyses of calcite to (1) characterize the nature and origin of the hydrothermal fluid and (2) determine the timing of the hydrothermal events responsible for gold mineralization.

2. Regional Background

The CTDs in the Dian–Qian–Gui area are distributed in the Nanpanjiang basin of the southwestern margin of the South China Block (Figure 1). The basin was initially developed in Devonian through rifting from the southwestern Yangtze Block. It evolved into a passive continental margin setting in the Early Carboniferous-Early Permian, a back-arc setting in late Permian, and a foreland basin setting in Early-Middle Triassic [28]. The exposed strata in the northwestern part of the basin primarily comprise shallow-water platform carbonates interbedded with sandstone, calcareous siltstone, and Permian Emeishan flood basalt. In the basin's southeastern segment, the strata mainly exhibit the deep-water basinal sequence of mudstone, siltstone, siliceous rocks, and micrite [29]. Two episodes of subduction-related tectonic events of the Paleo-Tethyan and Paleo-Pacific oceans have affected the sedimentation and deformation of the Nanpanjiang basin, forming a series of NE- and NW-striking faults and folds in the Nanpanjiang basin [30,31].

Igneous rocks in the Nanpanjiang basin are rare, the sporadically exposed rocks include the ~260 Ma Permian Emeishan basalt in the northern region of the basin, ~140–130 Ma quartz porphyry dykes in the central portion [32], and ~88–85 Ma lamprophyre dykes in the southeastern region [33].

3. Ore Deposit Geology

The Lannigou gold deposit (also known as Jinfeng) is the second-largest gold deposit in the Nanpanjiang basin [28]. It is located on the eastern flank of the NNE-trending Laizhishan anticline in the northern portion of the Nanpanjiang basin (Figure 2). The exposed strata in the ore district comprise Upper Carboniferous to Permian thick-bedded carbonate rocks (e.g., limestone, dolomitic limestone, bioclastic limestone, and reef limestone) and Triassic terrigenous clastic rocks, which from the bottom to the top include the Xuman, Niluo, Bianyang, and Luolou formations [7,26,34]. Gold mineralization is mainly hosted in the third and fourth subunits of the fourth Middle Triassic Xuman Formation ($T_2xm^{4\text{-}3}$ and $T_2xm^{4\text{-}4}$) unit and the Middle Triassic Bianyang Formation (T_2by) (Figure 2). The major rocks in the third subunit of the fourth Xuman Formation unit include calcareous mudstone, dolomitic siltstone, and sandstone, while the fourth unit comprises sandstone and argillite [8]. The Bianyang Formation is composed of sandstone, siltstone, and argillite.

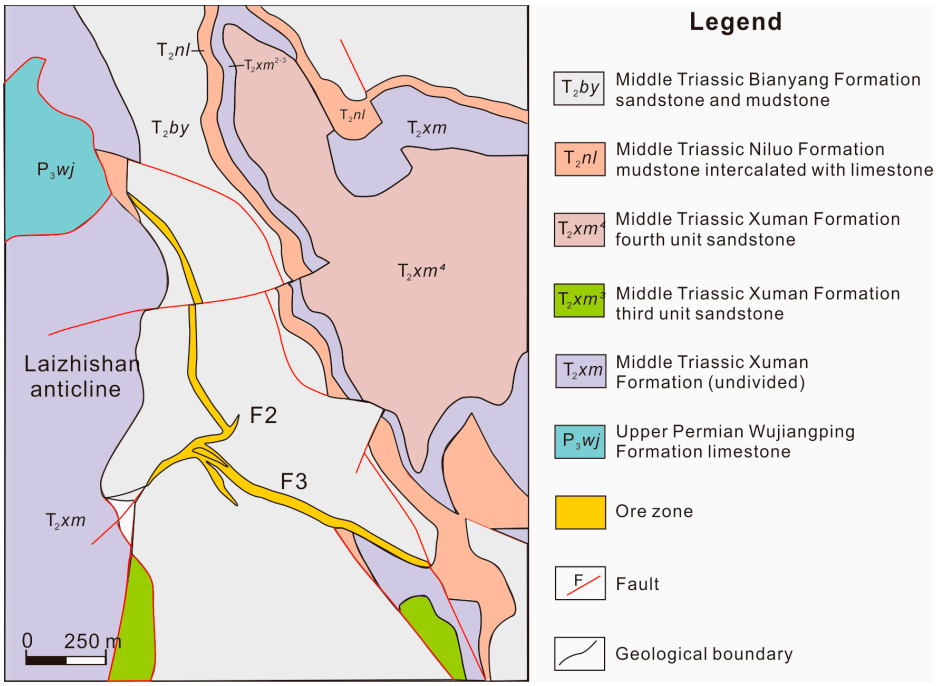

Figure 2. Geology map of the Lannigou gold deposit (modified after [3]).

Orebodies in the Lannigou gold deposit occur primarily as lenses and veins. They are strongly controlled by the NW- and NE-trending F_2, F_3, and F_6 fault zones, with the F_3 fault zone controlling ~80% of the Au reserves in the deposit [30,35]. Gold in the deposit is ionically bound in arsenian pyrite and arsenopyrite [34,36]. Hydrothermal alteration in the Lannigou deposit includes decarbonatization, silicification, dolomitization, argillization, and sulfidation. Three stages of minerals have been identified based on mineral paragenesis and crosscutting relationships [27,34,36]. The early-stage minerals are generally milky white vein quartz and relatively coarse, anhedral to euhedral pyrite, with nil to very low gold concentrations. These minerals are locally fractured and cemented by main- and late-stage minerals. Main-stage minerals comprise tiny arsenian pyrite, arsenopyrite, and marcasite enclosed by jasperoid quartz or disseminated in quartz-calcite. The late-stage minerals contain locally crosscut quartz, calcite, realgar, and orpiment or enclosed early- and main-stage minerals [3,37]. Magmatic rocks in the mining district are absent; the nearest rocks are the Baiceng ultramafic to mafic dykes (84 ± 1 Ma, SHRIMP zircon U-Pb) [38] ~25–30 km NNE of the mine.

Calcites are present in the main- and late-stage mineralization. Based on mineral assemblage and the cross-cutting relationship, three types of calcites have been identified from the Lannigou gold deposit (Figure 3): (1) type-I calcite (Cal-1) is white, smoky-gray, or pale-yellow and widely distributed in main-stage ores and altered wall rocks. It typically occurs as calcite–quartz–pyrite–arsenopyrite veins or veinlets cut through by type-II (Cal-2) and type-III (Cal-3) calcites. (2) Cal-2 is white and occurs as veins within the F_3 fault zones. This type of calcite generally fills structural cracks or vugs and is closely associated with high-maturity bitumen. (3) Cal-3 is milk-white and coexists with realgar, orpiment, stibnite, and quartz. No gold-bearing pyrite or arsenopyrite exists in this type of calcite vein.

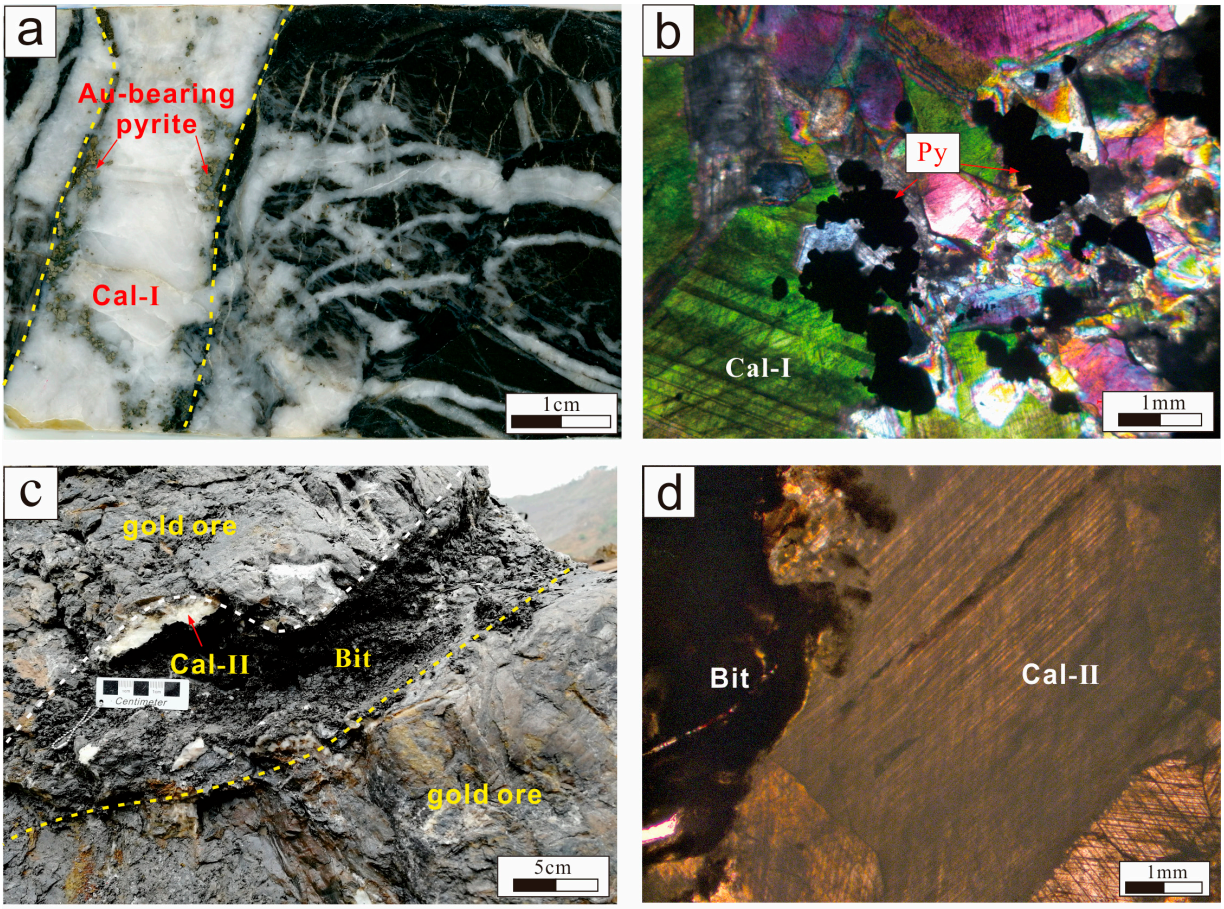

Figure 3. *Cont.*

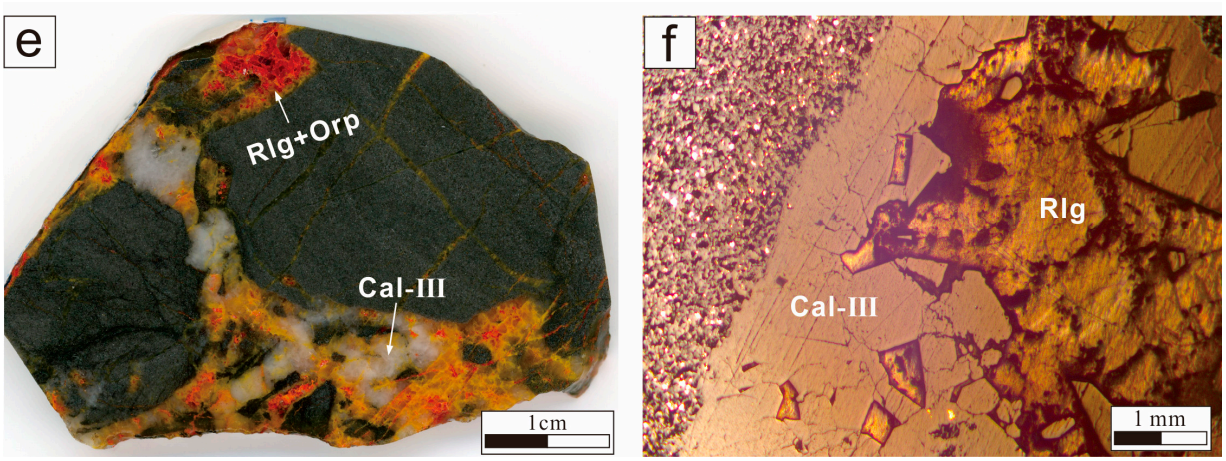

Figure 3. Representative hand specimen and microscopic photos of three calcite types from the Lannigou gold deposit. (**a**,**b**) Type-I calcite coexists with Au-bearing pyrite. (**c**,**d**) Type-II calcite intergrow with solid bitumen that cut through gold ores. (**e**,**f**) Type-III calcite coexists with realgar and orpiment. Mineral abbreviations: Bit-bitumen, Cal-calcite, Orp-orpiment, Rlg-realgar.

4. Analytical Methods

Three types of calcite samples were collected from calcite veins in the Lannigou gold deposit. Before Sm–Nd and C-O-Sr isotopic analysis, calcite grains were handpicked under a binocular microscope to ensure 99% purity and then powdered to 200 mesh in an agate mortar.

4.1. In-Situ Trace Element of Calcite

Calcite trace elements were analyzed at the State Key Laboratory of Ore Deposit Geochemistry, Institute of Geochemistry, Chinese Academy of Sciences, using an Agilent 7900 Inductively Coupled Plasma Mass Spectrometer (ICP-MS) coupled to a New Wave NWR femtosecond laser ablation system. Analyses were performed with a spot diameter of 50 μm and a repetition rate of 5 Hz. Helium was applied as a carrier gas, mixed with Argon via a T-connector before entering the ICP-MS. Each analysis included an 18 s background signal followed by 40 s data acquisition from the sample. The NIST 610, NIST 612, and MACS-3 standards were used for reference and quality control. The raw data were processed using the ICPMSDataCal program [39].

4.2. Sm–Nd Dating

Sm–Nd isotopic analyses were conducted at the Guizhou Tongwei Analytical Technology Co., Ltd., Guizhou, China, using the Nu Plasma HR Multi-Collector Inductively Coupled Plasma Mass Spectrometer (MC-ICP-MS). For detailed analytical procedures, please refer to [24]. The Nd ratio was normalized to a $^{146}Nd/^{143}Nd$ ratio of 0.7219. The standard materials, BHVO-2 and W-2a, were used for quality control and yielded $^{146}Nd/^{143}Nd$ ratios of 0.512990 ± 8 and 0.512518 ± 7, respectively, consistent with their recommended values of 0.512979 ± 14 and 0.512519 ± 15, demonstrating the reliability of our data. The average blanks were 0.03 ng for Sm and 0.05 ng for Nd. The decay constant of $\lambda^{147}Sm = 6.54 \times 10^{-12}$/year was adopted in the age calculation. The Sm–Nd isochron ages were plotted using the Isoplot/Ex_ver4.15 program [40].

4.3. C-O-Sr Isotope

Calcite C and O isotopic compositions were analyzed at Guizhou Tongwei Analytical Technology Co., Ltd. and Kunming University of Science and Technology. During analysis, an appropriate amount of calcite powder was weighed and reacted with 100% phosphoric acid at 90 °C for 4 h. The released CO_2 was measured on a stable isotope mass spectrometer (IsoPrime 100) [25]. The C isotope was reported in per mil (‰) relative to Vienna-Pee Dee

Belemnite (V-PDB); the O isotope was reported in per mil (‰) relative to Vienna-Standard Mean Ocean Water (V-SMOW). Analytical precision was considered > 0.2‰.

The calcite Sr isotopes were measured at Guizhou Tongwei Analytical Technology Co., Ltd. Based on the Sr content, ~50–100 mg calcite powders were dissolved with a mixture of concentrated nitric acid and hydrofluoric acid in a bomb at 185 °C. The digested solution was dried on a hot plate at 80 °C, mixed with 3 mL of 2 N nitric acid, and processed via column chemistry to separate Sr, following a previously reported protocol [41]. The Sr isotopes were analyzed on a VG Sector 54 thermal ionization mass spectrometer (TIMS). The raw data were corrected assuming an $^{86}Sr/^{88}Sr$ ratio = 0.1194. The standard materials, BHVO-2 and W-2a, were simultaneously prepared and measured, resulting in $^{87}Sr/^{86}Sr$ ratios of 0.703488 ± 10 and 0.706985 ± 11, respectively, consistent with their recommended values of 0.703478 ± 34 and 0.706965 ± 37 (http://georem.mpch-mainz.gwdg.de/, accessed on 15 February 2016).

5. Results

5.1. Trace and Rare Earth Elements

The trace and REE contents for the three types of calcites are presented in Supplementary Table S1. These calcites are generally enriched in Mg, Na, Fe, Mn, Sr, Si, Ba, and Y. Other trace elements, such as Al, K, Sc, Ti, V, Co, Ni, Zn, As, Pb, Th, and U, are low or below the detection limit. Compared to Cal-1 and Cal-2, Cal-3 has relatively lower Mn and Sr contents but higher As and Zr contents (Table S1).

The total REE of the three types of calcites is highly varied, with ∑REE contents of 5.28–31.2 ppm for Cal-1, 8.24–51.6 ppm for Cal-2, and 2.24–63.1 ppm for Cal-3. In the chondrite-normalized diagram, Cal-1 and Cal-2 display similar REE patterns with remarkable enrichment of middle rare earth elements (MREE: Sm-Ho) and depletion of light rare earth elements (LREE: La-Nd) and heavy rare earth elements (HREE: Er-Lu) (Figure 4). However, Cal-3 is depleted of LREE and enriched in MREE and HREE (Figure 4). Moreover, Cal-1 and Cal-2 exhibit apparent positive Eu anomalies with Eu/Eu* values of 1.51–4.48 and 2.57–8.33, respectively, whereas Cal-3 has a slightly negative Eu anomaly (Eu/Eu* = 0.66–0.91).

5.2. Sm–Nd Age

The Sm–Nd isotopic data for the calcites are listed in Table 1. Calcites from the calcite–quartz–pyrite–arsenopyrite veins (i.e., Cal-1) have $^{147}Sm/^{144}Nd$ and $^{143}Nd/^{144}Nd$ values ranging from 0.3303 to 0.5199 and 0.512115 to 0.512381, respectively. They yield a Sm–Nd isochron age of 213 ± 7 Ma (Figure 5a), with a low mean square of weighted deviates (MSWD) of 0.81, and an initial $^{143}Nd/^{144}Nd$ ratio of 0.511653 ± 0.000019. Calcites that coexist with bitumens (i.e., Cal-2) have $^{147}Sm/^{144}Nd$ and $^{143}Nd/^{144}Nd$ ratios of 0.4695–0.5992 and 0.512394–0.512555, respectively, yielding an Sm–Nd isochron age of 188 ± 14 Ma (Figure 5b), with an MSWD value of 0.34 and initial $^{143}Nd/^{144}Nd$ ratio of 0.511818 ± 0.000047.

Table 1. Sm/Nd isotope data for type-I and type-II calcites from the Lannigou gold deposit.

Sample No.	Description	Sm (ppm)	Nd (ppm)	$^{147}Sm/^{144}Nd$	±2σ	$^{143}Nd/^{144}Nd$	±2σ
LNG19-1	Type-I	0.9303	1.0812	0.519853	0.003088	0.512381	0.000009
LNG19-6-2	Type-I	5.3762	7.2388	0.448713	0.003656	0.512276	0.000004
LNG19-7-2	Type-I	4.8090	8.7972	0.330270	0.002674	0.512115	0.000003
LNG20-13	Type-I	0.9622	1.1732	0.495510	0.006161	0.512347	0.000006
LNG19-2	Type-II	0.4169	0.4735	0.531897	0.008338	0.512469	0.000015
LNG19-3-8	Type-II	2.0803	2.0978	0.599153	0.006612	0.512555	0.000006
LNG19-10	Type-II	2.3352	3.0049	0.469517	0.004504	0.512394	0.000006
LNG20-12	Type-II	1.8248	2.3074	0.477800	0.006522	0.512409	0.000005

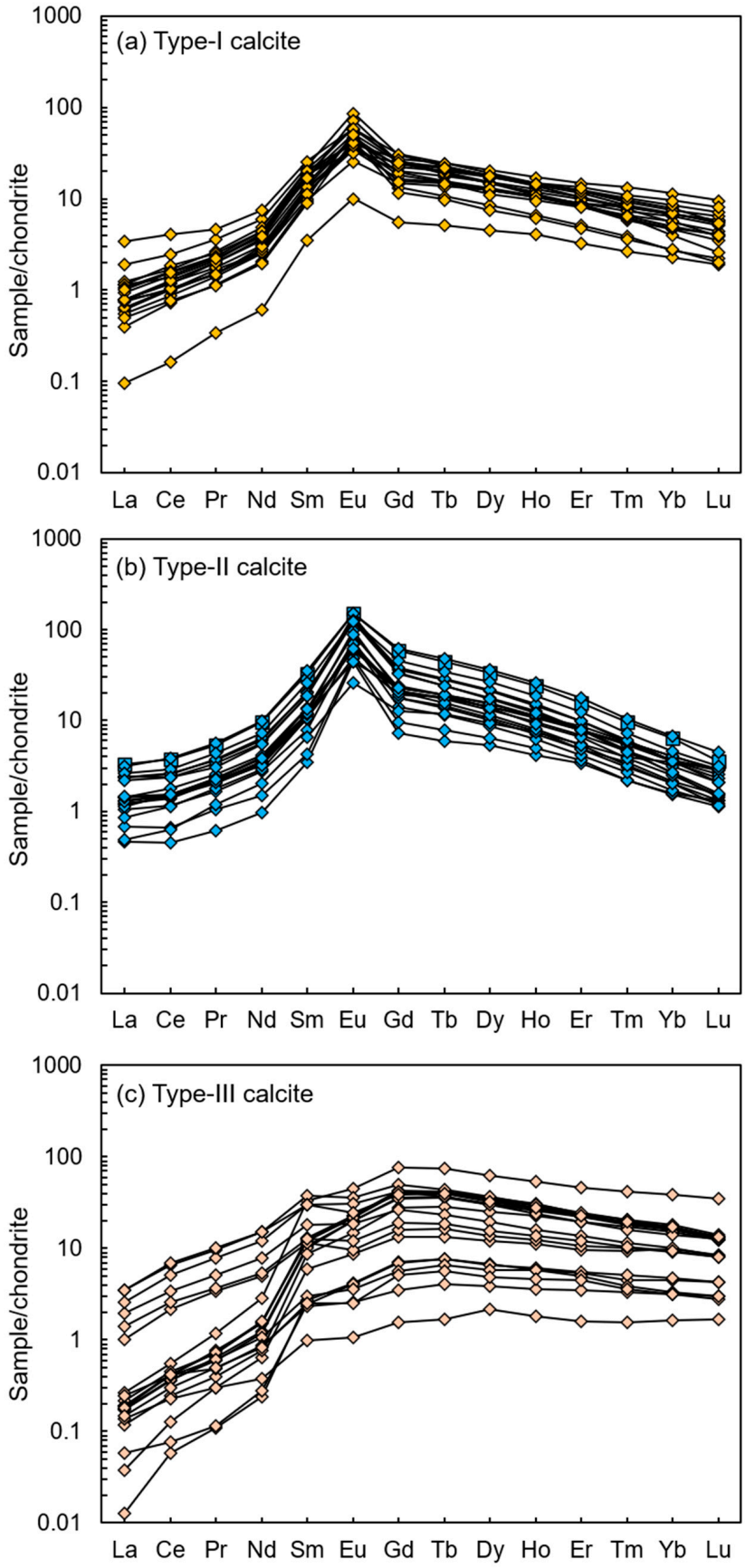

Figure 4. Chondrite-normalized REE patterns for the three types of calcites from the Lannigou gold deposit. The chondrite values were obtained from [42].

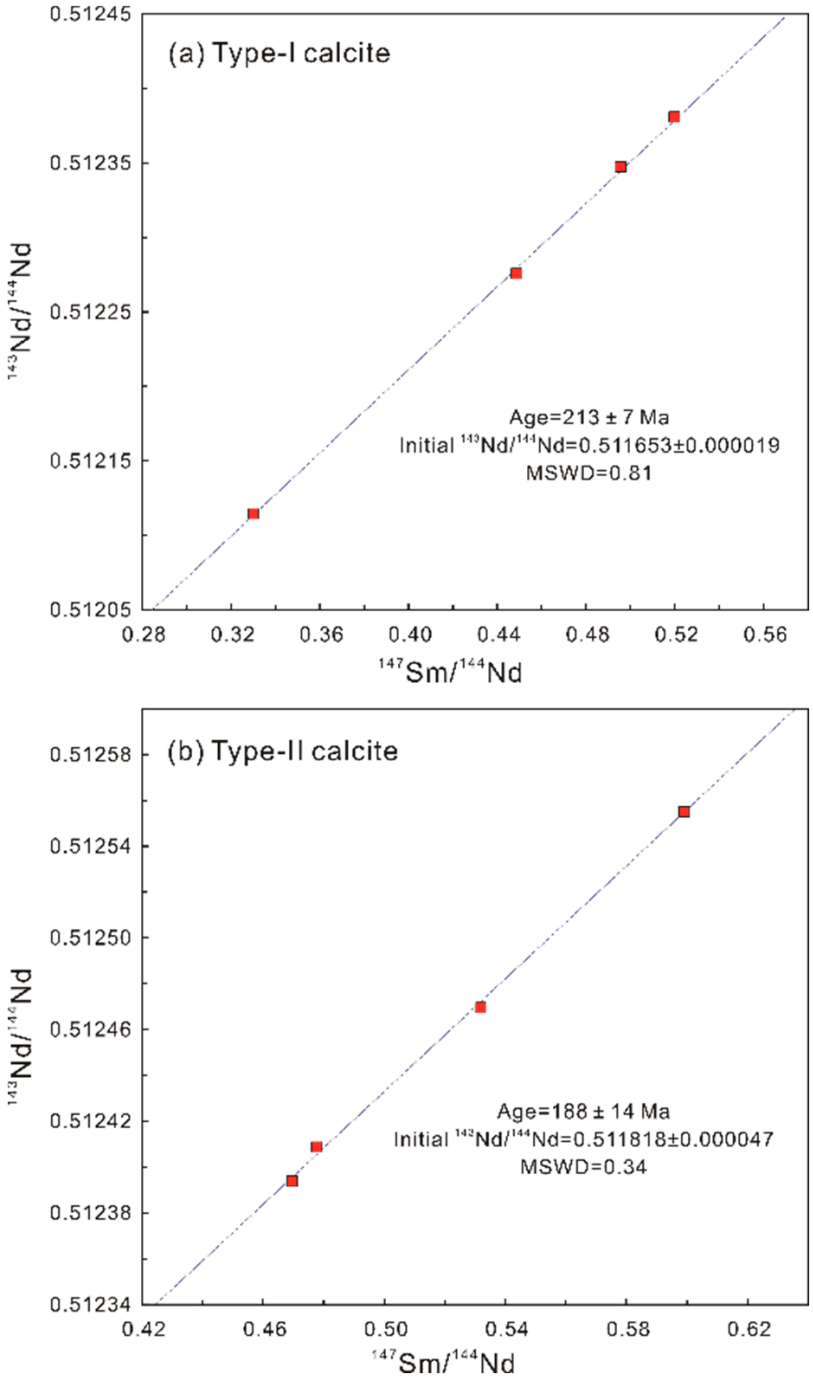

Figure 5. Sm–Nd isochrons for (**a**) type-I and (**b**) type-II calcites from the Lannigou gold deposit.

5.3. C-O-Sr Isotope

The C, O, and Sr isotopic composition of the three calcite types are presented in Table 2. Cal-1 and Cal-2 have similar $\delta^{13}C_{VPDB}$ and $\delta^{18}O_{VSMOW}$ values ranging from −2.3 to −0.9‰ (mean = −1.8‰, n = 14) and 6.3 to 19.9‰ (mean = 12.7‰, n = 14), respectively. These largely overlap with previous reported C-O isotopic data for the calcites from the Carlin-type gold deposits in the Nanpanjiang basin (Figure 6). Compared to Cal-1 and Cal-2, Cal-3 exhibits lower $\delta^{13}C_{VPDB}$ values of −4.4 to −2.2‰ (mean = −3.1‰, n = 6) but higher $\delta^{18}O_{VSMOW}$ values of 14.8 to 23.5‰ (mean = 20.5‰, n = 6) (Figure 6). The Sr isotopes of three types of calcite have a relatively small variation range, with $^{87}Sr/^{86}Sr$ values of 0.710155–0.710892 for Cal-1, 0.709183–0.709856 for Cal-2, and 0.708613–0.709547 for Cal-3.

Table 2. Carbon, oxygen, and strontium isotope data for the three types of calcites from the Lannigou gold deposit.

Sample No.	Description	$\delta^{13}C_{V\text{-}PDB}$ (‰)	$\delta^{18}O_{V\text{-}SMOW}$ (‰)	$\delta^{18}O_{fluid}$ (‰)	$^{87}Sr/^{86}Sr$	±2σ
LNG19-1	Type-I calcite	−2.0	12.6	2.83	0.710155	0.000010
LNG19-6-2	Type-I calcite	−1.6	10.7	0.93	0.710456	0.000010
LNG19-7-2	Type-I calcite	−1.3	9.5	−0.27	0.710892	0.000009
LNG20-13	Type-I calcite	−1.6	16.5	6.73		
LNG20-7	Type-I calcite	−1.2	7.2	−2.57		
LNG20-8	Type-I calcite	−2.3	6.3	−3.47		
LNG20-5	Type-I calcite	−1.8	13.1	3.33		
LNG19-2	Type-II calcite	−2.2	17.4	4.31	0.709856	0.000010
LNG19-3-8	Type-II calcite	−1.8	19.9	6.81	0.709183	0.000010
LNG19-10	Type-II calcite	−1.7	18.2	5.11	0.709787	0.000010
LNG20-12	Type-II calcite	−2.3	15.3	2.21		
LNG20-6	Type-II calcite	−1.6	9.9	−3.19		
LNG20-2	Type-II calcite	−2.3	11.9	−1.19		
LNG20-4	Type-II calcite	−0.9	8.7	−4.39		
LNG19-8	Type-III calcite	−3.1	22.0	8.91	0.709547	0.000011
LNG19-9-1a	Type-III calcite	−4.4	23.5	10.41	0.708613	0.000011
LNG19-9-1b	Type-III calcite	−4.0	22.7	9.61	0.708636	0.000009
LNG19-11	Type-III calcite	−3.0	20.0	6.91	0.709286	0.000011
LNG19-4	Type-III calcite	−2.2	20.4	7.31	0.709345	0.000010
LNG20-9	Type-III calcite	−2.2	14.8	1.71		

Note: $\delta^{18}O_{fluid}$(‰) = $\delta^{18}O_{V\text{-}SMOW\text{-}calcite}$ (‰)−1000Inαcalcite-water, 1000Inαcalcite-water = 4.01 × $10^6/T^2$ − 4.66 × 10^3/T + 1.71 [43], where the temperature (T) of 200 °C was assumed to the type-I calcite [26], and 150 °C was assumed to the type-II and type-III calcite [26,44].

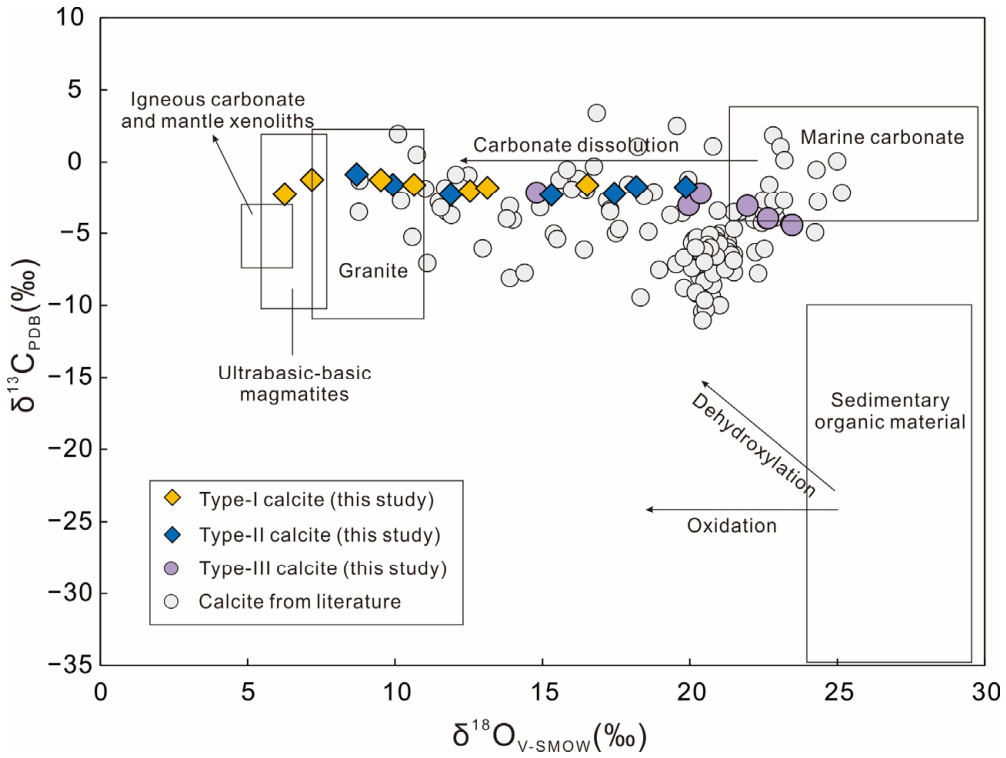

Figure 6. Carbon and oxygen isotopic compositions of calcite from the Carlin-type gold deposits in the Nanpanjiang basin. The base map is modified from [45], and the calcite data from the Carlin-type gold deposits in the literature were extracted from previous studies [15,25,26,46–49].

6. Discussion

6.1. Calcite Sm–Nd Ages Reveal Multiphase Hydrothermal Events in the Nanpanjiang Basin

The type-I and type-II calcites studied exhibit MREE-enriched patterns and high Sm/Nd ratios (0.55 to 0.99, Table 1) suitable for Sm–Nd dating [23,24,50]. Field and microscopic observations show that the type-I calcites are intergrown with Au-bearing arsenian pyrite (Figure 3a,b), indicating that the formation of Cal-1 is synchronous with gold deposition. Hence, the Sm–Nd isochron age of Cal-1 can represent the timing of gold mineralization at the Lannigou gold deposit. Here, the Cal-1 yields an isochron age of 213 ± 7 Ma, consistent with the previously reported arsenopyrite Re–Os ages (204 ± 19 Ma) [36], demonstrating the reliability of our obtained Sm–Nd age. The formation of ore-stage calcite is closely related to decarbonation and sulfidation processes during gold mineralization [3,5,16]. Recting metal-bearing hydrothermal fluid with Fe-riched calcareous host rocks will release sufficient iron and calcium from the wallrock into the ore-forming fluid, resulting in the precipitation of Au-bearing pyrite and calcite.

The type-II calcites are texturally associated with bitumens that cut through the gold orebody of the Lannigou gold deposit. Therefore, the Sm–Nd isochron age (188 ± 14 Ma, Figure 5b) of Cal-2 represents a post-ore hydrothermal event. Within uncertainty, this age is accordant with the Re–Os age (173 ± 6 Ma; [27]) of associated bitumens at the Lannigou, the Sm–Nd age (182 ± 21 Ma; [44]) of calcites from the Shitouzhai paleo-oil reservoir, and the U-Pb age (191.9 ± 2.2 Ma; [5]) of calcites (associated with bitumen) from the Shuiyindong gold deposit. Given the close temporal and paragenic relationship between Cal-2 and bitumen, we posit that the Sm–Nd age of Cal-2 represents a hydrocarbon accumulation event in the Nanpanjiang basin. Previous studies revealed two phases of hydrocarbon accumulation events in the Nanpanjiang basin [17,44]. Paleo-oil reservoirs derived from Devonian source rocks entered the oil window at the Late Paleozoic and cracked into bitumen in the Early-Middle Triassic [17], earlier than the ore-forming age of the Lannigou gold deposit. The Permian source rocks reached the oil window at the Middle-Late Triassic and cracked into high-maturity pyrobitumen and dry gas during the Early Jurassic (~173 Ma) [27]. This is consistent with our Cal-2 Sm–Nd age. Thus, we suggest that the Sm–Nd age of Cal-2 represents the thermal cracking age of crude oil derived from Permian source rocks.

As previously mentioned, the type-III calcites typically coexist with orpiment or realgar. Such a paragenetic association has been widely reported from the CTDs in the Nanpanjiang basin [5,24]. Early studies suggest that this mineral assemblage was precipitated in the late stage of Carlin-type gold mineralization. However, increasing evidence indicates that this hydrothermal event occurred ~150–130 Ma [5,22,24], approximately 60–80 Ma younger than the timing of gold mineralization. Huang [51] reported the U-Pb age of calcite from the orpiment–realgar–calcite veins at the Lannigou gold deposits, yielding a lower intercept age of 128.1 ± 4.6 Ma. This is consistent with the timing of hydrothermal activities recorded in other CTDs (e.g., Shuiyinding, Nibao, Zimudang, etc.) in the Nanpanjiang basin [52]. We interpret that this hydrothermal event may reflect the timing of arsenic remobilization from preexisting arsenian pyrite or arsenopyrite in the Early Cretaceous. High As contents in Cal-3 support this interpretation.

Based on our and previous results, three phases of hydrothermal fluid occurred in the Lannigou gold deposit: gold mineralization in the Late Triassic, oil cracking in the Early Jurassic, and arsenic remobilization in the Early Cretaceous. The existence of multiphase hydrothermal activities was not solely recorded in the Lannigou but also in other gold deposits in the Nanpanjiang basin, e.g., the Shuiyindong gold deposit [5,22], indicating that the Nanpanjiang basin may undergo multi-phase hydrothermal events in the Mesozoic.

6.2. Fluid Nature and Sources Responsible for the Precipitation of Calcites

REEs have similar geochemical behavior and are a useful proxy to trace fluid sources and paleohydrologic conditions of mineral precipitation [18]. REE^{3+} generally enters a calcite lattice via Ca^{2+} substitution. As the LREE has a closer ion radius to Ca^{2+} than HREE, most calcites in nature typically exhibit LREE-enriched and HREE-depleted patterns [53].

However, all three types of calcites studied were depleted in LREE and enriched in MREE (Figure 4), consistent with the REE patterns of ore-stage calcites from other CTDs (e.g., Shuiyindong, Zhesang, Zimudang) in the Nanpanjiang basin [24,25]. The REE pattern of calcite is influenced by co-precipitated minerals, Fe-Mn contents, and the hydrothermal fluid composition [19,54]. The co-precipitated minerals with calcites at the Lannigou mainly include quartz, arsenian pyrite, arsenopyrite, realgar, and orpiment (Figure 3), none of which are major REE carriers. Although previous studies found minor apatites in the CTDs, this mineral exhibits MREE-enriched and LREE-/HREE-depleted patterns [55,56]. Precipitation of apatite from hydrothermal fluid could not have accounted for the MREE-enriched patterns for our studied calcites. Meanwhile, incorporating Fe- and Mn-bearing micro-particles during calcite growth would lead to MREE- and HREE-enriched patterns due to the preferential absorption of MREE and HREE Fe-/Mn-bearing micro-particles [54]. However, Fe+Mn contents did not correlate with MREE/LREE or HREE/LREE ratios (Figure 7), indicating that the incorporation of Fe-/Mn-bearing micro-particles did not cause the presence of MREE-enriched patterns. Thus, we infer that the MREE-enriched feature of calcites was inherited from a hydrothermal fluid with an MREE-enriched composition or reacted with an MREE-enriched geological body before calcite precipitation.

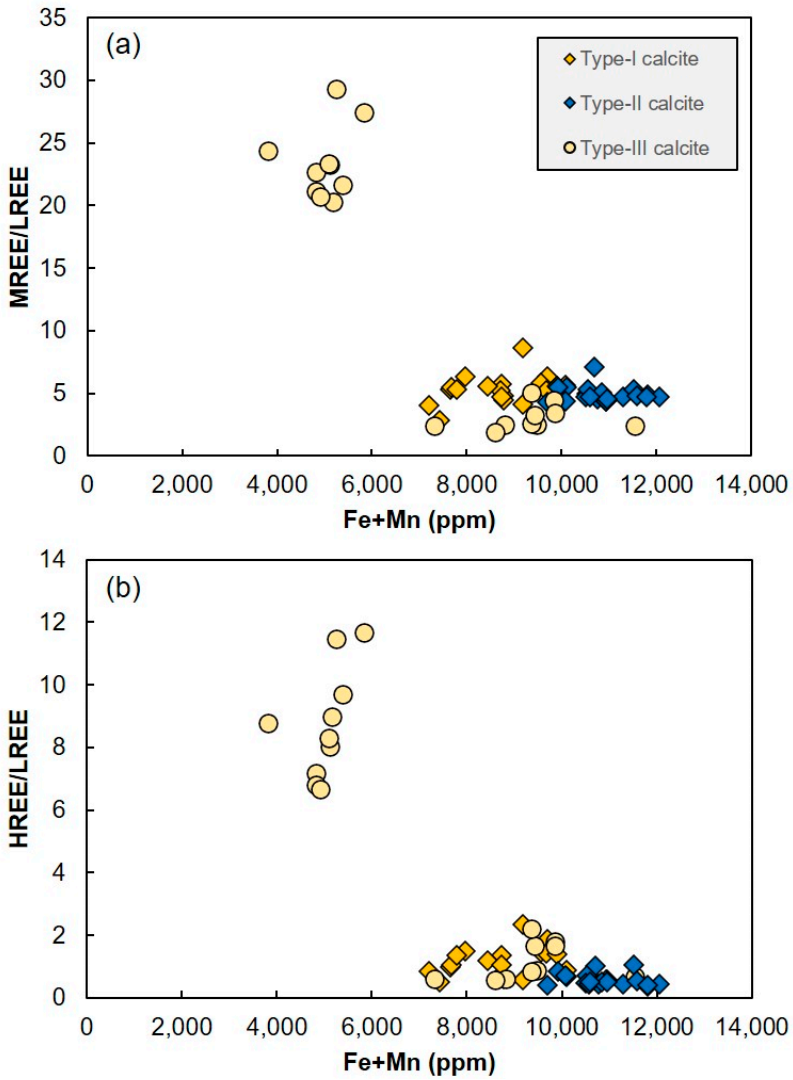

Figure 7. Plots of (**a**) Fe + Mn vs. MREE/LREE and (**b**) Fe + Mn vs. HREE/LREE for the three types of calcites from the Lannigou gold deposit.

The REE patterns of calcite can indicate fluid sources [57,58]. The three types of calcites from the Lannigou gold deposit exhibited MREE-enriched patterns (Figure 4), inconsistent with the calcites formed in magmatic-hydrothermal environments (e.g., skarn and carbonatite deposits), which are typically enriched in LREE [19,20]. However, the three calcite sample types were comparable to the LREE-depleted patterns in orogenic-style gold deposits [59], implying that our studied calcites may precipitate from metamorphic-related fluid. H-O isotopes support this inference that the CTD hydrothermal fluid primarily comprised metamorphic fluids mixed with meteoric water [3]. Thermodynamic modeling and theoretical calculations suggest that temperature is the most important parameter controlling the Eu^{3+}/Eu^{2+} redox potential in the hydrothermal fluid [60,61]. When the fluid temperature is >250 °C, Eu^{2+} dominates over Eu^{3+} in hydrothermal fluid and may be readily substituted for Ca^{2+}, leading to a positive Eu anomaly in precipitated minerals [58,59]. However, fluid inclusion microthermometry indicates that the homogenization temperature of the hydrothermal fluid in the Lannigou gold deposit is typically <250 °C [3,34], precluding temperature as a significant factor causing the positive Eu normally in our studied calcites. The Lannigou gold deposit is hosted in Triassic siliciclastic rocks; hydrothermal fluid inevitably reacted with those country rocks. The breakdown of plagioclase in clastic country rocks in response to the interaction with hydrothermal fluid could represent a dominant mechanism underlying our observed positive Eu normally in Cal-1 and Cal-2 [19]. In contrast, Cal-3 exhibits slightly negative Eu anomalies, which may reflect limited fluid–rock interactions.

Carbon, oxygen, and strontium isotopes can provide important constraints on fluid sources and calcite precipitation mechanisms [20]. The three types of calcites had narrow $\delta^{13}C$ variations of −4.4 to 0.9‰, well within the range of marine carbonates (Figure 6). Hence, the carbon in calcites primarily originated from regional Paleozoic marine carbonate. Using the method proposed by Zheng [43], the $\delta^{18}O$ of water ($\delta^{18}O_{H2O}$) in equilibrium with type-I and type-II calcites yielded similar $\delta^{18}O_{H2O}$ values of −3.47 to 6.73‰ (mean = 1.07‰) and −4.39 to 6.81‰ (mean = 1.38‰), respectively. These values primarily overlap with the metamorphic fluid (3 to 25‰) [60], with fewer values within the range of meteoric water (−7 to −14‰) [3] in the Nanpanjiang basin. This suggests that the hydrothermal fluid related to the formation of these two types of calcites is derived from a mixed fluid source of metamorphic fluid and meteoric water. Compared to the type-I and type-II calcites, the fluid equilibrium of type-III calcites exhibited high $\delta^{18}O_{H2O}$ values of 1.71 to 10.41‰ (mean = 7.47‰). This may indicate a metamorphic fluid source with a limited contribution of meteoric water. The three types of calcites all had high Sr content and low Rb content and Rb/Sr ratio (Table S1). Thus, the radiogenic ^{87}Sr accumulation by ^{87}Rb decay is limited in the present-day calcite Sr isotope composition [57]. That is, the measured $^{87}Sr/^{88}Sr$ values of calcite can approximately represent the Sr isotopic composition of hydrothermal fluid. Calcites from the Lannigou gold deposit have $^{87}Sr/^{86}Sr$ values of 0.708613–0.710892, higher than the $^{87}Sr/^{86}Sr$ values of the Paleozoic–Triassic country rock and Permian mafic rocks. In this case, a higher $^{87}Sr/^{86}Sr$ reservoir may have contributed to the hydrothermal fluid. Previous studies have shown that the Neoproterozoic basement rocks in the margin of the Nanpanjiang basin have a high $^{87}Sr/^{86}Sr$ composition (0.757851–0.766069) [61]. Therefore, we infer that the higher $^{87}Sr/^{86}Sr$ source may originate from concealed basement rocks in the Nanpanjiang basin.

6.3. Implication for Fluid Evolution, Metal Mineralization, and Hydrocarbon Accumulation

The Nanpanjiang basin is located in the hinge area of the Paleo-Tethys and Paleo-Pacific tectonic domains. Its formation and evolution are closely related to the subduction and closure of the Paleo-Tethys and Paleo-Pacific oceans. In response to the opening and development of the Ailaoshan-Song Ma Paleo-Tethys ocean in the Late Paleozoic, the Nanpanjiang basin deposited thick (>3000 m) marine carbonate and organic-bearing shale and mudstone in a passive continental margin environment [62,63]. These organic-bearing sedimentary rocks typically have high organic carbon abundances (TOCs) of

0.37%–3.63% [64]. They are enriched in metals (e.g., Au, As, Hg, Sb) that act as source rocks for the latter gold mineralization and hydrocarbon accumulation [44,65,66]. Due to the subduction and closure of the Paleo-Tethys Ocean, the South China Block collided with the Indochina Block in the Early to Middle Triassic. This collision event (i.e., Indosinian orogeny) may trigger large-scale circulation of basin fluid that leached ore-forming metals from source rocks. The Au-bearing ore-forming fluid migrated along pre-existing faults and reacted with Fe-rich minerals (e.g., Fe-dolomite) in wall rocks [3,24], resulting in metal precipitation via sulfidation and forming the type-I calcites in the Late Triassic. Meanwhile, the Indosinian orogeny resulted in rapid subsidence of the Nanpanjiang basin and deposited ~6000 clastic rocks in the Triassic [63]. This caused the Paleozoic hydrocarbon source rocks to reach the oil windows and generate liquid oil [63,64,67]. In the Early Jurassic, these accumulated oil reservoirs began thermal cracking to form high-maturity bitumen as recorded in the bitumen Re–Os (173 ± 6 Ma) [27] and Sm–Nd age (188 ± 14 Ma in this study) of the type-II calcites. In the Late Jurassic-Early Cretaceous, the low-angle subduction of the Paleo-Pacific Ocean again drove fluid circulation in the Nanpanjiang basin, forming significant arsenic and antimony mineralization [5]. This is accordant with the development of 145 Ma Sb deposits (e.g., Qinglong) in the Nanpanjiang basin [21]. The type-III calcites, which coexisted with realgar and orpiment, have Sm–Nd and U–Pb ages of ~130–150 Ma [5,24], also consistent with this interpretation. Due to the lack of direct evidence of Cal-3- and Au-bearing minerals, the genetic links between Late Jurassic-Early Cretaceous hydrothermal events and gold mineralization are unclear and warrant further investigation.

7. Conclusions

(1) The Nanpanjiang basin experienced multi-phase hydrothermal fluid events in the Mesozoic. The first event was genetically related to gold mineralization in the Late Triassic, the second was associated with the hydrocarbon thermal cracking in the Early Jurassic, and the third occurred in the Early Cretaceous and was related to arsenic and antimony mineralization.

(2) The REE patterns and C-O isotopes of calcites suggest that the type-I and type-II calcites were derived from a mixed fluid source of metamorphic fluid and meteoric water. In contrast, the type-III calcite was mainly precipitated from metamorphic fluid with no or little contribution from meteoric water.

(3) Calcite C-O-Sr isotopes indicate that the carbon in the hydrothermal fluid was mainly sourced from marine carbonate, and strontium was primarily from the regional metamorphic basement.

(4) Basin fluid evolution, gold mineralization, and hydrocarbon accumulation in the Nanpanjiang basin are closely related to the Indosinian and Yanshanian orogenies due to the collision of the South China Block with the Indochina Block and the flat subduction of Paleo-Pacific Ocean.

Supplementary Materials: The following supporting information can be downloaded at: https://www.mdpi.com/article/10.3390/min13111420/s1, Table S1: In-situ trace element composition of three types of calcites from the Lannigou gold deposit.

Author Contributions: P.L. and Y.H. wrote the manuscript. Y.H. designed this project. S.G., Z.T. and H.F. helped interpret the data. All authors have read and agreed to the published version of the manuscript.

Funding: This work was supported by the National Natural Science Foundation of China (NSFC) (grants no. 41672073) and the Entrusted Project of China Gold Group Jinfeng Mining Co., Ltd. (no. 2020FW86).

Data Availability Statement: All the data are presented in the paper.

Conflicts of Interest: The authors declare no conflict of interest.

References

1. Cline, J.S.; Hofstra, A.H.; Muntean, J.L.; Tosdal, R.M.; Hickey, K.A.; Hedenquist, J.W.; Thompson, J.F.H.; Goldfarb, R.J.; Richards, J.P. Carlin-type gold deposits in Nevada: Critical geologic characteristics and viable models. In *Economic Geology. 100th Anniversary Volume*; Society of Economic Geologists: Littleton, CO, USA, 2005; pp. 451–484.
2. Frimmel, H.E. Earth's continental crustal gold endowment. *Earth Planet. Sci. Lett.* **2008**, *267*, 45–55. [CrossRef]
3. Su, W.; Dong, W.; Zhang, X.; Shen, N.; Hu, R.; Hofstra, A.H.; Cheng, L.; Xia, Y.; Yang, K. Carlin-type gold deposits in the Dian-Qian-Gui "Golden Triangle" of Southwest China. *Econ. Geol.* **2018**, *20*, 157–185.
4. Hu, R.; Fu, S.; Huang, Y.; Zhou, M.-F.; Fu, S.; Zhao, C.; Wang, Y.; Bi, X.; Xiao, J. The giant South China Mesozoic low-temperature metallogenic domain: Reviews and a new geodynamic model. *J. Asian Earth Sci.* **2017**, *137*, 9–34. [CrossRef]
5. Jin, X.-Y.; Zhao, J.-X.; Feng, Y.-X.; Hofstra, A.H.; Deng, X.-D.; Zhao, X.-F.; Li, J.-W. Calcite U-Pb dating unravels the age and hydrothermal history of the giant Shuiyindong Carlin-type gold deposit in the golden triangle, South China. *Econ. Geol.* **2021**, *116*, 1253–1265. [CrossRef]
6. Gao, W.; Hu, R.; Hofstra, A.H.; Li, Q.; Zhu, J.; Peng, K.; Mu, L.; Huang, Y.; Ma, J.; Zhao, Q. U-Pb dating on hydrothermal rutile and monazite from the Badu gold deposit supports an early Cretaceous age for Carlin-type gold mineralization in the Youjiang Basin, Southwestern China. *Econ. Geol.* **2021**, *116*, 1355–1385. [CrossRef]
7. Gao, W.; Hu, R.; Huang, Y.; Zhu, J.; Li, Q.; Mei, L.; Bi, X.; Liu, J. Hydrothermal apatite as a robust U–Th–Pb chronometer for the Carlin-type gold deposits in the Youjiang basin, SW China. *Miner. Depos.* **2023**. [CrossRef]
8. Xie, Z.; Xia, Y.; Cline, J.S.; Pribil, M.J.; Koenig, A.; Tan, Q.; Wei, D.; Wang, Z.; Yan, J. Magmatic origin for sediment-hosted Au deposits, Guizhou Province, China: In situ chemistry and sulfur isotope composition of pyrites, Shuiyindong and Jinfeng deposits. *Econ. Geol.* **2018**, *113*, 1627–1652. [CrossRef]
9. Wei, D.-T.; Zhou, T.-F.; Xia, Y.; Fan, Y.; Xie, Z.-J.; Liu, X.-J.; Tan, Q.-P.; Bai, L.-A.; Wang, F.-Y. Pyrite textural, trace elemental and sulfur isotope signatures of the Badu gold deposit, Youjiang basin (SW China): Implications for ore-fluid source and Au precipitation mechanism. *Ore Geol. Rev.* **2022**, *149*, 105083. [CrossRef]
10. Hou, L.; Peng, H.; Ding, J.; Zhang, J.; Zhu, S.; Wu, S.; Wu, Y.; Ouyang, H. Textures and in situ chemical and isotopic analyses of pyrite, Huijiabao trend, Youjiang Basin, China: Implications for paragenesis and source of sulfur. *Econ. Geol.* **2016**, *111*, 331–353. [CrossRef]
11. Xie, Z.; Huang, K.-J.; Xia, Y.; Cline, J.; Tan, Q.; Liu, J.; Xiao, J.; Yan, B. Heavy δ^{26}Mg values in carbonate indicate a magmatic-hydrothermal origin of Carlin-type Au deposit. *Geochim. Cosmochim. Acta* **2022**, *333*, 166–183. [CrossRef]
12. Wang, Q.; Groves, D. Carlin-style gold deposits, Youjiang Basin, China: Tectono-thermal and structural analogues of the Carlin-type gold deposits, Nevada, USA. *Miner. Depos.* **2018**, *53*, 909–918. [CrossRef]
13. Cline, J.S.; Muntean, J.L.; Gu, X.X.; Xia, Y. A Comparison of Carlin-type gold deposits: Guizhou Province, Golden Triangle, Southwest China, and northern Nevada, USA. *Earth Sci. Front.* **2013**, *20*, 1–18.
14. Hu, R.Z.; Su, W.C.; Bi, X.W.; Tu, G.Z.; Hofstra, A.H. Geology and geochemistry of Carlin-type gold deposits in China. *Miner. Depos.* **2002**, *37*, 378–392.
15. Peng, Y.; Gu, X.; Zhang, Y.; Liu, L.; Wu, C.; Chen, S. Ore-forming process of the Huijiabao gold district, southwestern Guizhou Province, China: Evidence from fluid inclusions and stable isotopes. *J. Asian Earth Sci.* **2014**, *93*, 89–101. [CrossRef]
16. Su, W.; Heinrich, C.A.; Pettke, T.; Zhang, X.; Hu, R.; Xia, B. Sediment-hosted gold deposits in Guizhou, China: Products of wall-rock sulfidation by deep crustal fluids. *Econ. Geol.* **2009**, *104*, 73–93. [CrossRef]
17. Gu, X.X.; Li, B.H.; Xu, S.H.; Fu, S.H.; Dong, S.Y. Characteristics of hydrocarbon-bearing ore-forming fluids in the Youjiang basin, South China: Implication for hydrocarbon accumulation and ore mineralization. *Earth Sci. Front.* **2007**, *24*, 133–146.
18. Debruyne, D.; Hulsbosch, N.; Muchez, P. Unraveling rare earth element signatures in hydrothermal carbonate minerals using a source–sink system. *Ore Geol. Rev.* **2016**, *72*, 232–252. [CrossRef]
19. Myint, A.Z.; Wagner, T.; Fusswinkel, T. Calcite trace element geochemistry of Au deposits in the Singu-Tabeikkyin Gold District, Myanmar: Implications for the sources of ore-forming fluids. *Ore Geol. Rev.* **2022**, *145*, 104892. [CrossRef]
20. Yan, S.; Niu, H.-C.; Zhao, J.-X.; Bao, Z.-W.; Sun, W.D. Ore-fluid geochemistry and metallogeny of the Dunde iron–zinc deposit in western Tianshan, Xinjiang, China: Evidence from fluid inclusions, REE and C–O–Sr isotopes of calcite. *Ore Geol. Rev.* **2018**, *100*, 441–456. [CrossRef]
21. Peng, J.-T.; Hu, R.-Z.; Jiang, G.-H. Samarium-Neodymium isotope system of fluorites from the Qinglong antimony deposit, Guizhou Province: Constraints on the mineralizing age and ore-forming materials' sources. *Acta Petrol. Sin.* **2003**, *19*, 785–791.
22. Tan, Q.; Xia, Y.; Xie, Z.; Wang, Z.; Wei, D.; Zhao, Y.; Yan, J.; Li, S. Two hydrothermal events at the Shuiyindong carlin-type gold deposit in Southwestern China: Insight from Sm–Nd dating of fluorite and calcite. *Minerals* **2019**, *9*, 230. [CrossRef]
23. Tonguç Uysal, I.; Zhao, J.-X.; Golding, S.D.; Lawrence, M.G.; Glikson, M.; Collerson, K.D. Sm–Nd dating and rare-earth element tracing of calcite: Implications for fluid-flow events in the Bowen Basin, Australia. *Chem. Geol.* **2007**, *238*, 63–71. [CrossRef]
24. Su, W.; Hu, R.; Xia, B.; Xia, Y.; Liu, Y. Calcite Sm–Nd isochron age of the Shuiyindong Carlin-type gold deposit, Guizhou, China. *Chem. Geol.* **2009**, *258*, 269–274. [CrossRef]
25. Wang, J.; Chang, J.; Li, C.; Han, Z.; Wang, T.; Han, H. Significance of calcite trace elements contents and C-O Isotopic compositions for ore-forming fluids and gold prospecting in the Zhesang Carlin-like gold deposit of Southeastern Yunnan, China. *Minerals* **2020**, *10*, 338. [CrossRef]

26. Zhuo, Y.; Hu, R.; Xiao, J.; Zhao, C.; Huang, Y.; Yan, J.; Li, J.; Gao, W.; Li, J. Trace elements and C-O isotopes of calcite from Carlin-type gold deposits in the Youjiang Basin, SW China: Constraints on ore-forming fluid compositions and sources. *Ore Geol. Rev.* **2019**, *113*, 103067. [CrossRef]
27. Li, P.Y.; Guan, S.J.; Hu, Y.Z.; Tian, Z.D.; Cheng, Y.; Wang, X.L.; Tan, X.L.; Zhou, L. Origin and Re-Os geochronology of vein bitumen in the Nanpanjiang basin, SW China: Implication for the ore-forming age of Carlin-type gold deposits. *Ore Geol. Rev.* **2022**, *149*, 105118. [CrossRef]
28. Du, Y.S.; Huang, H.; Yang, J.H.; Huang, H.W.; Tao, P.; Huang, Z.Q.; Hu, L.S.; Xie, C.X. The basin translation from Late Paleozoic to Triassic of the Youjiang basin and its tectonic signification. *Geol. Rev.* **2013**, *59*, 1–11, (In Chinese with English Abstract).
29. Zheng, L.J.; Tan, Q.P.; Zuo, Y.J.; Xia, Y.; Xie, Z.J.; Zheng, L.L.; Liu, J.Z. Two hydrothermal events associated with Au mineralization in the Youjiang Basin, southwestern China. *Ore Geol. Rev.* **2022**, *144*, 104816. [CrossRef]
30. Hu, Y.; Liu, W.; Zhang, G.; Guan, S.; Lu, Y.; Li, P.; Zheng, S.; Fan, H.; Betts, P.G. Seismic reflection profiles reveal the ore-controlling structures of Carlin-style gold deposits in Lannigou gold fields, Southwestern Guizhou, China. *Econ. Geol.* **2022**, *117*, 1203–1224. [CrossRef]
31. Liu, Y.; Hu, K.; Han, S.; Sun, Z. Structural evolution of the Youjiang basin and its controlling effects on the formation of Carlin-type gold deposits. *Geol. J. China Univ.* **2015**, *21*, 1.
32. Zhu, J.-J.; Hu, R.-Z.; Richards, J.P.; Bi, X.-W.; Stern, R.; Lu, G. No genetic link between Late Cretaceous felsic dikes and Carlin-type Au deposits in the Youjiang basin, Southwest China. *Ore Geol. Rev.* **2017**, *84*, 328–337. [CrossRef]
33. Liu, S.; Su, W.; Hu, R.; Feng, C.; Gao, S.; Coulson, I.M.; Wang, T.; Feng, G.; Tao, Y.; Xia, Y. Geochronological and geochemical constraints on the petrogenesis of alkaline ultramafic dykes from southwest Guizhou Province, SW China. *Lithos* **2010**, *114*, 253–264. [CrossRef]
34. Zhang, X.-C.; Spiro, B.; Halls, C.; Stanley, C.J.; Yang, K.-Y. Sediment-hosted disseminated gold deposits in southwest Guizhou, PRC: Their geological setting and origin in relation to mineralogical, fluid inclusion, and stable isotope characteristics. *Int. Geol. Rev.* **2003**, *45*, 407–470. [CrossRef]
35. Chen, M.; Mao, J.; Frank, P.B.; Tony, N.; Phillip, J.U. Structural features and metallogenesis of the Carlin-type Jinfeng (Lannigou) gold deposit, Guizhou Province, China. *Ore Geol. Rev.* **2011**, *43*, 217–234.
36. Chen, M.; Mao, J.; Li, C.; Zhang, Z.; Dang, Y. Re–Os isochron ages for arsenopyrite from Carlin-like gold deposits in the Yunnan–Guizhou–Guangxi "golden triangle", southwestern China. *Ore Geol. Rev.* **2015**, *64*, 316–327. [CrossRef]
37. Yan, J.; Mavrogenes, J.A.; Liu, S.; Coulson, I.M. Fluid properties and origins of the Lannigou Carlin-type gold deposit, SW China: Evidence from SHRIMP oxygen isotopes and LA-ICP-MS trace element compositions of hydrothermal quartz. *J. Geochem. Explor.* **2020**, *215*, 106546. [CrossRef]
38. Chen, M.H.; Zhang, W.; Yang, Z.X.; Lu, G.; Hou, K.J.; Liu, J.H. Zircon SHRIMP U- Pb age and Hf isotopic composition of Baiceng ultrabasic dykes in Zhenfeng County, southwestern Guizhou Province. *Miner. Depos.* **2009**, *28*, 240–250.
39. Liu, Y.; Gao, S.; Hu, Z.; Gao, C.; Zong, K.; Wang, D. Continental and oceanic crust recycling-induced melt–peridotite interactions in the Trans-North China Orogen: U–Pb dating, Hf isotopes and trace elements in zircons from mantle xenoliths. *J. Petrol.* **2010**, *51*, 537–571. [CrossRef]
40. Ludwig, K.R. *User's Manual for Isoplot 3.00, a Geochronological Toolkit for Microsoft Excel*; Berkeley Geochronology Center Special Publication: Berkeley, CA, USA, 2003; pp. 25–32.
41. Deniel, C.; Pin, C. Single-stage method for the simultaneous isolation of lead and strontium from silicate samples for isotopic measurements. *Anal. Chim. Acta* **2001**, *426*, 95–103. [CrossRef]
42. Sun, S.S.; McDonough, W.F. Chemical and isotopic systematics of oceanic basalts: Implications for mantle composition and processes. *Geol. Soc. Lond. Spec. Publ.* **1989**, *42*, 313–345. [CrossRef]
43. Zheng, Y.F. Oxygen isotope fractionation in carbonate and sulfate minerals. *Geochem. J.* **1999**, *33*, 109–126. [CrossRef]
44. Gu, X.X.; Zhang, Y.M.; Li, B.H.; Dong, S.Y.; Xue, C.J.; Fu, S.H. Hydrocarbon- and ore-bearing basinal fluids: A possible link between gold mineralization and hydrocarbon accumulation in the Youjiang basin, South China. *Miner. Depos.* **2012**, *47*, 663–682. [CrossRef]
45. Liu, J.; He, M.; Li, Z.; Liu, Y.; Li, C.; Zhang, Q.; Yang, W.; Yang, A. Oxygen and carbon isotopic geochemistry of Baiyangping silver-copper polymetallic ore concentration area in Lanping basin of Yunnan province and its significance. *Miner. Depos.* **2004**, *23*, 1–9.
46. Tan, Q.P.; Xia, Y.; Wang, X.Q.; Xie, Z.J.; Wei, D.T. Carbon-oxygen isotopes and rare earth elements as an exploration vector for Carlin-type gold deposits: A case study of the Shuiyindong gold deposit, Guizhou Province, SW China. *J. Asian Earth Sci.* **2017**, *148*, 1–12. [CrossRef]
47. Jin, X.Y. Geology, Mineralization and Genesis of the Nibao, Shuiyindong and Yata Gold Deposits in SW Guizhou Province, China. Ph.D. Thesis, China University of Geoscience, Wuhan, China, 2017. (In Chinese with English Abstract)
48. Guo, Z.C. The geological feature and origin of the Zimudang gold deposit in Xingren County, Guizhou Province. *Guizhou Geol.* **1998**, *5*, 201–218. (In Chinese with English Abstract)
49. Wang, Z.P.; Xia, Y.; Song, X.Y.; You, B.; Zheng, X.H.; Wang, X.Y. Isotope and REE characteristics and ore-forming materials source of the Taipingdong–Zimudang gold deposit. *Acta Mineral. Sin.* **2012**, *32*, 93–100. (In Chinese with English Abstract)
50. Peng, J.T.; Hu, R.Z.; Burnard, P.G. Samarium–neodymium isotope systematics of hydrothermal calcites from the Xikuangshan antimony deposit (Hunan, China): The potential of calcite as a geochronometer. *Chem. Geol.* **2003**, *200*, 129–136. [CrossRef]

51. Huang, Y. Mineralization Age and Material Source of the Carlin-Type Gold Deposits in Southwestern Guizhou. Ph.D. Thesis, Institute of Geochemistry, Chinese Academy of Sciences, Guiyang, China, 2019; p. 180.
52. Huang, Y.; Hu, R.; Bi, X.; Fu, S.; Peng, K.; Gao, W.; Oyebamiji, A.; Zhaanbaeva, A. Low-temperature thermochronology of the Carlin-type gold deposits in southwestern Guizhou, China: Implications for mineralization age and geological thermal events. *Ore Geol. Rev.* **2019**, *115*, 103178. [CrossRef]
53. Perry, E.; Gysi, A.P. Hydrothermal calcite-fluid REE partitioning experiments at 200 °C and saturated water vapor pressure. *Geochim. Cosmochim. Acta* **2020**, *286*, 177–197. [CrossRef]
54. Wang, J.; Wen, H.; Fan, H.; Zhu, J. Sm-Nd geochronology, REE geochemistry and C and O isotope characteristics of calcites and stibnites from the Banian antimony deposit, Guizhou Province, China. *Geochem. J.* **2012**, *46*, 393–407. [CrossRef]
55. Chen, M.; Bagas, L.; Liao, X.; Zhang, Z.; Li, Q. Hydrothermal apatite SIMS Th-Pb dating: Constraints on the timing of low-temperature hydrothermal Au deposits in Nibao, SW China. *Lithos* **2019**, *324–325*, 418–428. [CrossRef]
56. Wei, D.-T.; Zhou, T.-F.; Xia, Y.; Chen, J.; Xie, Z.-J.; Liu, X.-J.; Pang, B.-C.; Tan, Q.-P.; Bai, L.-A. Ore fluid origin recorded by apatite chemistry: A case study on altered dolerite from the Badu Carlin-type gold deposit, Youjiang basin, SW China. *Ore Geol. Rev.* **2022**, *143*, 104745. [CrossRef]
57. Liu, G.; Yuan, F.; Deng, Y.; Wang, F.; White, N.C.; Huizenga, J.M.; Li, Y.; Li, X.; Zhou, T. Ore-fluid geochemistry of the Hehuashan Pb–Zn deposit in the Tongling ore district, Anhui province, China: Evidence from REE and C–H–O isotopes of calcite. *Ore Geol. Rev.* **2020**, *117*, 103279. [CrossRef]
58. Graf, J.L., Jr. Effects of mississippi valley-type mineralization on REE patterns of carbonate rocks and minerals, Viburnum trend, Southeast Missouri. *J. Geol.* **1984**, *92*, 307–324. [CrossRef]
59. Kalliomäki, H.; Wagner, T.; Fusswinkel, T.; Schultze, D. Textural evolution and trace element chemistry of hydrothermal calcites from Archean gold deposits in the Hattu schist belt, eastern Finland: Indicators of the ore-forming environment. *Ore Geol. Rev.* **2019**, *112*, 103006. [CrossRef]
60. Kesler, S.E. Ore-forming fluids. *Elements* **2005**, *1*, 13–18. [CrossRef]
61. Peng, B.; Robert, F.; Tu, X. Nd-Sr-Pb isotopic geochemistry of scheelite from the Woxi W-Sb-Au deposit, western Hunan: Implications for sources and evolution of ore-forming fluids. *Acta Geol. Sin.* **2006**, *8*, 561–570.
62. Liu, Y.; Hu, K.; Han, S.; Sun, Z. The characteristics of organic matter and its relationship with the formation of Carlin-type gold deposits in Southwest Guizhou Province. *Geochemica* **2016**, *45*, 281–302.
63. Ge, X.; Selby, D.; Liu, J.; Chen, Y.; Cheng, G.; Shen, C. Genetic relationship between hydrocarbon system evolution and Carlin-type gold mineralization: Insights from ReOs pyrobitumen and pyrite geochronology in the Nanpanjiang Basin, South China. *Chem. Geol.* **2021**, *559*, 119953. [CrossRef]
64. Zhao, M.J.; Zhang, S.C.; Zhao, L.; Liu, P.C. Geochemistry and genesis of bitumen in Paleo-oil reservoir in the Nanpanjiang basin, China. *Acta Geol. Sin.* **2006**, *80*, 893–901.
65. Gu, X.; Zhang, Y.; Li, B.; Xue, C.; Dong, S.; Fu, S.; Cheng, W.; Liu, L.; Wu, C. The coupling relationship between metallization and hydrocarbon accumulation in sedimentary basins. *Earth Sci. Front.* **2010**, *17*, 83–105. (In Chinese with English Abstract)
66. Gu, X.X.; Li, B.H.; Xu, S.H.; Fu, S.H.; Dong, S.Y. Analysis of the charge history of the Shitouzhai Permian paleo-oil reservoir, Guizhou, SW China: Fluid inclusion and Sm-Nd isotope constraints. *Acta Petro. Sin.* **2007**, *23*, 2279–2286. (In Chinese with English Abstract)
67. Ge, X.; Shen, C.; He, P.; Jin, Y.; Li, S.; Chen, Y. The roles of hydrocarbons on the mineralization of Carlin-type gold deposits, Nanpanjiang Basin, South China. *Ore Geol. Rev.* **2022**, *149*, 105107. [CrossRef]